

## Polar mesospheric clouds formed from space shuttle exhaust

Michael H. Stevens,<sup>1</sup> Jörg Gumbel,<sup>2</sup> Christoph R. Englert,<sup>1</sup> Klaus U. Grossmann,<sup>3</sup> Markus Rapp,<sup>4</sup> and Paul Hartogh<sup>5</sup>

Received 4 March 2003; revised 22 April 2003; accepted 5 May 2003; published 31 May 2003.

[1] We observe a plume of water vapor in the Arctic above 85 km and a day after an August shuttle launch. Our satellite observations reveal that a discrete region of polar mesospheric clouds (PMCs) appears a week after that launch. We calculate that the water contained in the observed PMCs is consistent with the amount injected by the shuttle. This is evidence for a source of PMCs not previously considered. *INDEX TERMS*: 0320 Atmospheric Composition and Structure: Cloud physics and chemistry; 0341 Atmospheric Composition and Structure: Middle atmosphere—constituent transport and chemistry (3334); 0355 Atmospheric Composition and Structure: Thermosphere—composition and chemistry; 0360 Atmospheric Composition and Structure: Transmission and scattering of radiation. **Citation**: Stevens, M. H., J. Gumbel, C. R. Englert, K. U. Grossmann, M. Rapp, and P. Hartogh, Polar mesospheric clouds formed from space shuttle exhaust, *Geophys. Res. Lett.*, 30(10), 1546, doi:10.1029/2003GL017249, 2003.

### 1. Introduction

[2] The coldest region of the Earth's atmosphere is high above the summer pole, where temperatures fall below 130 K near 88 km. Under such frigid conditions, water vapor at a few parts per million by volume (ppmv) condenses to form polar mesospheric clouds (PMCs) observed near 82 km. These wispy ice clouds are not in the historical record prior to 1885, which has prompted speculation that they are indicators of global change initiated lower in the atmosphere [Thomas *et al.*, 1989].

[3] In this work, we propose that Arctic PMCs can be created from space shuttle water vapor exhaust injected into the upper atmosphere off the east coast of the United States. Our evidence is from Arctic observations by three different experiments. We first present satellite and ground-based observations of a plume above 85 km a day after launch. We then show that the amount of water sequestered in PMCs observed by satellite five days later is equivalent to that contained in the plume. We briefly discuss the implications to the interpretation of the historical PMC record.

### 2. The Observations

[4] On 7 August 1997 the space shuttle Discovery (STS-85) launched with the CRyogenic Infrared Spectrometers

and Telescopes for the Atmosphere-Shuttle Pallet Satellite (CRISTA-SPAS) in the payload bay. Later that day, CRISTA-SPAS was deployed to observe the Earth's atmosphere for eight days using two limb scanning instruments flying together for the second time. The Middle Atmosphere High Resolution Spectrograph Investigation (MAHRSI) measured both UV solar resonance fluorescence of OH and sunlight scattered from PMCs near 309 nm [Stevens *et al.*, 2001]. Above ~65 km, OH is produced predominantly by the photolysis of water vapor and therefore can be used as a water vapor proxy [Summers *et al.*, 2001]. CRISTA measured the infrared emissions of a variety of species between 4–71  $\mu\text{m}$  [Grossmann *et al.*, 2002] and PMCs near 12  $\mu\text{m}$ .

[5] Exhaust from the shuttle's main engines is almost entirely water vapor and for STS-85 ~44% (~300 metric tons) is injected between 108–114 km. This plume is about 1100 km long and stretches across ~7 degrees of latitude. It expands to a diameter of ~3 km before equilibrating to the ambient temperature and pressure [Vlasov and Grushin, 1996]. We use satellite OH observations from MAHRSI and ground-based microwave observations of water vapor to infer transport of this water following launch.

#### 2.1. Satellite Observations: Tracking the Plume

[6] Figure 1 shows OH and PMC observations from MAHRSI during this mission. The panels are assembled chronologically from data obtained between 0.9 and 7.2 days after launch. Each square represents a limb observation of OH emission, which includes contributions arising from above the indicated tangent altitude along the line-of-sight.

[7] Figure 1a shows a region of enhanced OH intensities measured near Greenland about 1.1 days after launch and peaking at  $44 \pm 2$  kR. This is nearly the same mission elapsed time and intensity as the plume observation from the first MAHRSI mission [Stevens *et al.*, 2002] suggesting that the enhanced emission also originates from the relocated shuttle plume. The reported mean wind near 110 km altitude in the summer for these latitudes is northward at 10–20 m/s [Wang *et al.*, 1997], whereas the required northward speed for the plume to reach Greenland is  $35 \pm 10$  m/s. The wind structure in this altitude region is known to be complex, however, with reported peak wind speeds in excess of 100 m/s 60% of the time and large shears below the maximum [Larsen, 2002].

[8] Figure 1b shows another region of bright intensities measured over Siberia the next day. The localized nature of this emission suggests it is from the same water vapor inferred in Figure 1a. Figures 1a and 1b together indicate that between 1.1–1.6 days after launch, this plume passed over a ground-based microwave spectrometer in Norway, indicated by the triangular symbol in Figure 1b.

<sup>1</sup>E.O. Hulburt Center for Space Research, Naval Research Laboratory, Washington, D.C., USA.

<sup>2</sup>Universities Space Research Association, Washington, D.C., USA.

<sup>3</sup>Department of Physics, University of Wuppertal, Wuppertal, Germany.

<sup>4</sup>Leibniz Institute of Atmospheric Physics e.V., Kühlungsborn, Germany.

<sup>5</sup>Max Planck Institute for Aeronomy, Katlenburg-Lindau, Germany.

## 2.2. Ground-Based Observations: Confirming Transport

[9] We now present water vapor observations from the microwave spectrometer located at 69°N and 16°E. The instrument [Hartogh and Jarchow, 1995] measures the spectral shape of the atmospheric water vapor emission at 22.235 GHz. Since the emissions from different altitude layers are pressure broadened, vertical profiles of water vapor can be retrieved from the observed line shape. The

instrument is normally sensitive to altitudes between about 35–85 km. Below 35 km the retrieval is limited by the spectrometer bandwidth of 40 MHz. Above ~85 km the Doppler broadening exceeds the pressure broadening and the spectrum contains no altitude information. The half-width at half-maximum of this feature is 25–30 kHz, comparable to the maximum resolution of the spectrometer (22 kHz).

[10] Figure 2 shows three spectra averaged over consecutive 20-minute intervals following launch of STS-85. The data are in brightness temperature (K) and so are proportional to the radiated power as defined by the Planck function. The middle panel shows that 1.3 days (31.8 hours) after launch, the signal originating above 85 km was enhanced by 500–700 milliKelvin (mK) where the measurement uncertainty ( $1\sigma$ ) is about 160 mK. Note that only the portion of the spectrum that yields information above 85 km is enhanced and that this enhancement occurs exactly when the satellite OH observations would imply. The total number of water vapor molecules that produce this signal is  $4 \pm 1 \times 10^{29}$  at 233 K, over 400 times the water vapor normally expected in our line-of-sight above 85 km. This is about 4% of the amount injected into the lower thermosphere by the shuttle, reasonably consistent with the field of view ( $40 \times 120$  km full-width at half-maximum) convolved with the plume dimensions. The average northward speed of the plume calculated from the launch time and this ground-based detection is  $31 \pm 4$  m/s, in agreement with MAHRSI observations. These ground-based observations therefore provide even more evidence that the shuttle plume was transported to the Arctic.

## 2.3. Arctic Descent and Ice Formation

[11] We now extrapolate the trajectory of the plume using mean wind observations. The estimated trajectory of the water vapor is shown as the solid line in Figure 1c. A mean eastward wind of 35–50 m/s [Fleming et al., 1996] is used for its transport between Figure 1b and the point of ice formation indicated in Figure 1c. The emission altitudes indicated in parentheses in Figures 1a–1c are calculated

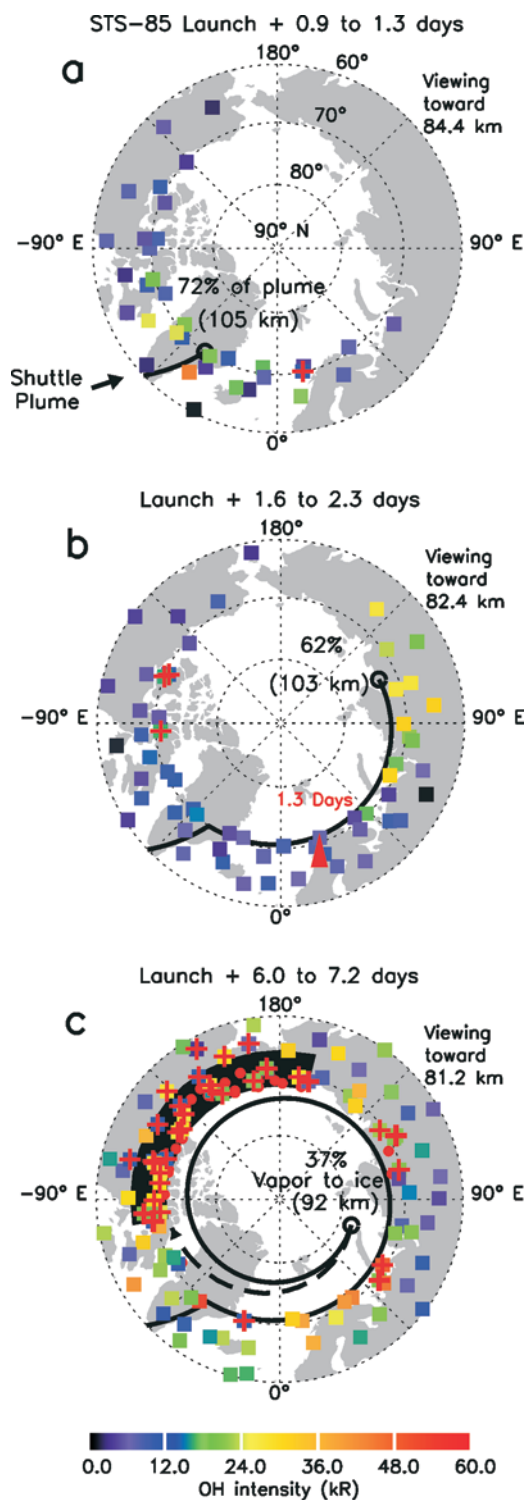


**Figure 1.** (opposite) The inferred path of STS-85 water exhaust injected near 111 km. Each colored square is the result of a 4.4 s integration over the 11 brightest OH features in MAHRSI spectra between 307.8–301.6 nm. Intensities are in kiloRayleighs measured viewing toward tangent altitudes indicated and PMC observations are shown as red crosses. a. The peak OH intensity near Greenland is measured 1.1 days after launch and the inferred plume path is shown as the solid black line. The inferred altitude of the plume is in parentheses next to the open circle and the percentage of remaining shuttle water vapor exhaust is indicated (see text). b. The plume moves eastward past a ground-based microwave spectrometer in Norway (red triangular symbol) and then over Siberia, where enhanced OH emission was measured by MAHRSI 1.6–1.8 days after launch. c. The plume is projected eastward around the pole and downward, forming ice near 92 km. The ice then moves southwest over North America as shown by the black dashed line. The PMCs are observed by both MAHRSI and CRISTA (red circles) near 81 km. The shaded region indicates the area used to calculate the total water content in the observed PMCs.

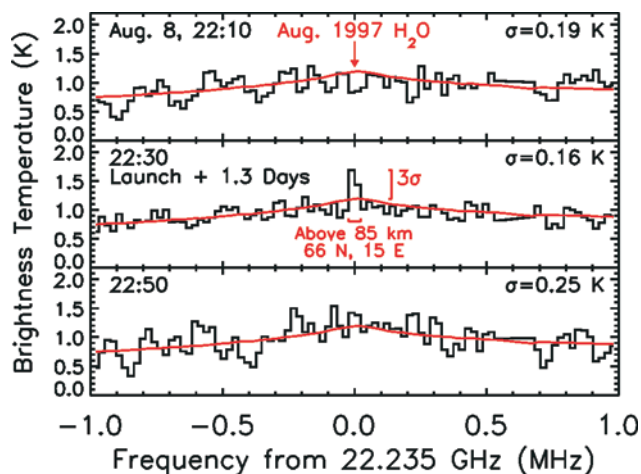


**Figure 2.** Microwave emission of water vapor measured from Andenes, Norway. Three consecutive 20-minute intervals of data are shown from top to bottom in black, with the signal from the STS-85 plume shown 1.3 days after launch. The spectrometer observes at an elevation angle of 18 degrees pointing south from its location at 69°N. The August, 1997 spectrum is shown for reference in red. The variation in the standard deviation ( $\sigma$ ) between panels is due to changes in the tropospheric contribution, which is subtracted from these data.

from descent rates of 5–6 cm/s, consistent with those reported for the Arctic summer by *Lieberman et al.* [2000].

[12] In general, growth of a water ice particle can proceed when the partial pressure of water vapor exceeds the saturation pressure of water vapor over ice. Photodissociation, discussed below, reduces the water vapor mixing ratio in the plume during its transport. The descending water vapor nonetheless remains extremely concentrated ( $>10^4$  ppmv) relative to its natural abundance when it reaches 92 km. Here the temperature is near 170 K [*Grossmann et al.*, 2002], which in combination with the high water concentration allows for ice formation [*Marti and Mauersberger*, 1993] at this pressure (0.09 Pa). These ice particles are about 10 km higher than normally observed and would not necessarily yield a peak in a limb scan of solar scattered light, where the brightest PMC signal is typically near 82 km.

[13] The zonal wind reversal indicated in Figure 1c agrees with observations and accompanies the predicted phase change from vapor to ice. The ice particles grow, fall and remain in the 82 km region, where the mean vertical wind is upward [*Rapp et al.*, 2002; *Lieberman et al.*, 2000] and horizontal winds are toward the southwest [*Mitchell et al.*, 2002].

[14] Figures 1a and 1b indicate few PMCs, in agreement with a climatology showing that the occurrence probability is less than 15% in mid-August between 70–75°N [*Thomas and Olivero*, 1989]. However, Figure 1c shows that both MAHRSI and CRISTA observed a concentrated patch of late season PMCs appearing over northern North America 6.1–7.2 days after launch [*Stevens et al.*, 2001]. Why did these clouds form? The localized OH and water vapor enhancements in the Arctic observed earlier in the mission point to a large and concentrated region of water vapor as the source. To further investigate whether shuttle exhaust is responsible for

these PMCs, we now quantify the amount of water they sequester.

### 3. Data Analysis

#### 3.1. PMC Thermal Emission

[15] Figure 3 shows CRISTA radiance profiles from the PMCs indicated by the filled circles in Figure 1c. Radiances are integrated between 11.70–11.90  $\mu\text{m}$ , where there is a peak in the water ice emission spectrum [*Witt*, 2001]. There is a clear surplus of emission near 82 km, which can be converted to an equivalent local water vapor density as follows.

[16] The optically thin thermal emission,  $L(T, \lambda)$ , measured from an ice cloud observed by CRISTA may be written

$$L(T, \lambda) = J(T, \lambda) \cdot I_c. \quad (1)$$

Here  $J(T, \lambda)$  is the source function at temperature  $T$  and wavelength  $\lambda$ .  $J(T, \lambda)$ , according to Kirchhoff's law, is the product of the Planck spectrum and the absorptivity of water ice [*Warren*, 1984].  $I_c$  is the total volume of ice measured along a column. The relationship between the thermal emission and the ice column is independent of the size distribution of the PMC particles. Solution of (1) requires the PMC temperature and the complex index of refraction for ice. We find that at 145 K [*Grossmann et al.*, 2002] the source function is  $0.0104 \text{ W cm}^{-3} \text{ sr}^{-1}$  for the spectral region indicated in Figure 3, which yields an ice column of  $9.6 \times 10^{-7} \text{ cm}^3/\text{cm}^2$ .

[17] The ice column can be expressed as

$$[H_2O] = \rho_{H_2O} \times I_c / (M_{H_2O} \times LOS) \quad (2)$$

where  $[H_2O]$  is the average number density ( $\text{cm}^{-3}$ ) of water ice,  $\rho_{H_2O}$  is the ice density ( $\text{g}/\text{cm}^3$ ),  $M_{H_2O}$  is the mass of a water molecule (g) and  $LOS$  is the line of sight through the cloud (cm). A homogeneous 1.0 km thick cloud layer viewed on the limb ( $LOS = 2.30 \times 10^7 \text{ cm}$ ) yields an average local water density of  $1.32 \times 10^9 \text{ cm}^{-3}$  at 82 km. The density is multiplied by the volume containing the observed PMCs in Figure 1c ( $3.10 \times 10^{21} \text{ cm}^3$ ) to find the water content of the ice layer observed over northern North America.

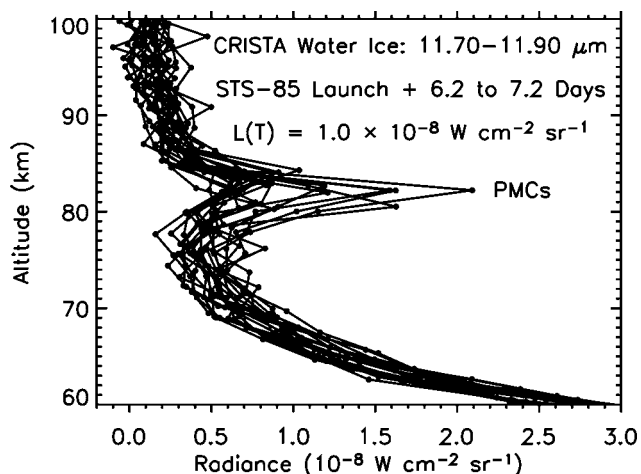


**Figure 3.** CRISTA water ice radiance profiles measured between August 13–14, 1997. The profiles are collected from the PMC observations in the shaded region of Figure 1c. The mean PMC radiance,  $L(T)$ , is calculated using an average of these 21 scans.

[18] We therefore calculate the total number of water molecules observed in the ice phase (the shaded area in Figure 1c) to be  $4.1 \times 10^{30} \pm 50\%$ . The uncertainty arises from the limited latitudinal extent of our observations, the cloud temperature and the approximated PMC thickness. The total is about 40% of the amount injected by the shuttle between 108–114 km, indicating that there is enough water vapor in the injected shuttle plume to form the PMCs indicated in Figure 1c. This is on average  $\sim 3.5$  ppmv and comparable to model predictions for water vapor there [Summers *et al.*, 2001; Berger and von Zahn, 2002]. Shuttle exhaust could therefore at least transiently contribute to the Arctic summer water budget near 82 km.

### 3.2. Loss of Plume Water Vapor

[19] We now calculate the water vapor loss during transport of the plume. We assume that the plume is entirely water vapor while descending to 92 km at which time it forms ice. We use a one-dimensional photochemical model [Summers *et al.*, 2001] with the varying lighting conditions during the transport implied by the solid line in Figure 1c. Under these conditions, the UV solar Lyman- $\alpha$  (Ly- $\alpha$ ) flux near 121.6 nm contributes to about 60% of the photodissociation on average for a fully illuminated plume. However, water vapor's cross-section to Ly- $\alpha$  is high enough [Lewis *et al.*, 1983] so that the plume can protect itself from this radiation. The effective opacity depends on the path length through the water vapor. A plume fully protected from Ly- $\alpha$  and optically thin to Ly- $\alpha$  are both considered as limiting cases.

[20] Also included in the loss calculation is the recombination of radicals to form water vapor following photodissociation [Körner and Sonnemann, 2001], which depends on how efficiently atomic oxygen is mixed into the plume. We consider both a pure water vapor plume and one that is mixed completely with atomic oxygen in our calculations.

[21] We find that between 19–61% of the water vapor injected by the shuttle remains upon ice formation in the Arctic, which we estimate to be four days after launch. This corresponds to a total of  $3.8 \times 10^{30} \pm 60\%$  water vapor molecules, indeed consistent with the amount inferred from the CRISTA PMC observations. This is quantitative evidence that the observed PMCs condensed directly from shuttle water vapor exhaust.

### 4. Summary

[22] By inferring transport of the shuttle plume from both satellite and ground-based observations and by comparing its water content to that sequestered in an unexpected region of Arctic ice clouds, we have shown evidence that shuttle exhaust can form PMCs. The ultimate fate of the water after our PMC observations would likely be influenced further by dynamics since it is much longer lived in the middle atmosphere, particularly as ice. Water is a common effluent in many propellant combinations. If the phenomenon we describe is repeatable for at least a subset of all rocket launches, PMC observations could be influenced by space traffic. We propose that this source be considered in the analysis of PMC trends. We furthermore suggest care be exercised when using the historical record of PMC observations as an indicator of global climate change initiated from the lower atmosphere.

[23] **Acknowledgments.** We thank D.E. Siskind, S.M. Bailey and R. R. Conway for many important discussions. J.G. Cardon, R. Spang, M. Ait Assou and Li Song provided valuable assistance with data analysis. This work was supported by the Office of Naval Research and the NASA Office of Space Science.

### References

- Berger, U., and U. von Zahn, Icy particles in the summer mesopause region: Three-dimensional modeling of their environment and two-dimensional modeling of their transport, *J. Geophys. Res.*, *107*, 1366, doi:10.1029/2001JA000316, 2002.
- Fleming, E. L., et al., Climatological mean wind observations from the UARS high-resolution Doppler imager and wind imaging interferometer: Comparison with current reference models, *J. Geophys. Res.*, *101*, 10,455–10,473, 1996.
- Grossmann, K. U., The CRISTA-2 mission, *J. Geophys. Res.*, *107*, 8173, doi:10.1029/2001JD000667, 2002.
- Hartogh, P., and C. Jarchow, Groundbased detection of middle atmospheric water vapor, *Proc. SPIE*, *2586*, 188–195, 1995.
- Körner, U., and G. R. Sonnemann, Global three-dimensional modeling of the water vapor concentration of the mesosphere-mesopause region and implications with respect to the noctilucent cloud region, *J. Geophys. Res.*, *106*, 9639–9651, 2001.
- Larsen, M. F., Winds and shears in the mesosphere and lower thermosphere: Results from four decades of chemical release wind measurements, *J. Geophys. Res.*, *107*, doi:10.1029/2001JA000218, 2002.
- Lewis, B. R., et al., The aeronomical dissociation of water vapor by solar H Lyman  $\alpha$  radiation, *J. Geophys. Res.*, *88*, 4935–4940, 1983.
- Lieberman, R. S., et al., Comparison of mesospheric and lower thermospheric residual wind with High Resolution Doppler Imager, medium frequency, and meteor radar winds, *J. Geophys. Res.*, *105*, 27,023–27,035, 2000.
- Marti, J., and K. Mauersberger, A survey and new measurements of ice vapor pressure at temperatures between 170 and 250 K, *Geophys. Res. Lett.*, *20*, 363–366, 1993.
- Mitchell, N. J., et al., Mean winds and tides in the Arctic mesosphere and lower thermosphere, *J. Geophys. Res.*, *107*, 1004, doi:10.1029/2001JA900127, 2002.
- Rapp, M., et al., Small scale temperature variations in the vicinity of NLC: Experimental and model results, *J. Geophys. Res.*, *107*, 4392, doi:10.1029/2001JD001241, 2002.
- Stevens, M. H., et al., PMCs and the water frost point in the Arctic summer mesosphere, *Geophys. Res. Lett.*, *28*, 4449–4452, 2001.
- Stevens, M. H., et al., OH observations of space shuttle exhaust, *Geophys. Res. Lett.*, *29*, 1378, doi:10.1029/2002GL015079, 2002.
- Summers, M. E., et al., Discovery of a water vapor layer in the Arctic summer mesosphere: Implications for polar mesospheric clouds, *Geophys. Res. Lett.*, *28*, 3601–3604, 2001.
- Thomas, G. E., and J. J. Olivero, Climatology of polar mesospheric clouds 2. Further analysis of Solar Mesosphere Explorer data, *J. Geophys. Res.*, *94*, 14,673–14,681, 1989.
- Thomas, G. E., et al., Relation between increasing methane and the presence of ice clouds at the mesopause, *Nature*, *338*, 490–492, 1989.
- Vlasov, M. N., and V. V. Grushin, A model of global distribution of the exhaust gases from rocket engines in the upper atmosphere, *Cosmic Res.*, *34*, 30–35, 1996.
- Wang, D. Y., et al., Empirical model of 90–120 km horizontal winds from wind-imaging interferometer green line measurements in 1992–1993, *J. Geophys. Res.*, *102*, 6729–6745, 1997.
- Warren, S. G., Optical constants of ice from the ultraviolet to the microwave, *Appl. Opt.*, *23*, 1206–1225, 1984.
- Witt, G., Thermal properties and thermodynamic limitations of the size of noctilucent cloud particles, *Proc. 15th ESA Symposium on European Rocket and Balloon Programmes and Related Research ESA SP-471*, 231, 2001.

M. H. Stevens and C. R. Englert, Code 7641, Naval Research Laboratory, 4555 Overlook Ave., SW, Washington, DC, 20375 USA. (stevens@uap2.nrl.navy.mil)

J. Gumbel, Department of Meteorology, Stockholm University, S-106 91, Stockholm, Sweden.

K. U. Grossmann, Department of Physics, University of Wuppertal, 42097 Wuppertal, Germany.

M. Rapp, Leibniz Institute of Atmospheric Physics e.V., 18225 Kühlungsborn, Germany.

P. Hartogh, Max Planck Institute for Aeronomy, 37191 Katlenburg-Lindau, Germany.